Smart Structures and Systems, *Vol. 26, No. 4* (*2020*) *507-520*
DOI: https://doi.org/10.12989/sss.2020.26.4.507

Exploratory research on ultra-long polymer optical fiber-based corrosion sensing for buried metal pipelines

Dong Luo[1a], Yuanyuan Li[1b], Hangzhou Yang[2c], Hao Sun[3,4d] and Hongbin Chen[*5]

[1]*School of Human Settlements and Civil Engineering, Xi'an Jiaotong University, Xi'an, Shaanxi, 710049, China*
[2]*School of Physics, Northwest University, Xi'an, Shaanxi, 710069, China*
[3]*Department of Civil and Environmental Engineering, Northeastern University, Boston, MA, 02115, USA*
[4]*Department of Civil and Environmental Engineering, MIT, Cambridge, MA, 02139, USA*
[5]*Department of Civil Engineering, Tsinghua University, Beijing, 100084, China*

(*Received January 30, 2020, Revised April 28, 2020, Accepted June 11, 2020*)

Abstract. In order to achieve effective corrosion monitoring of buried metal pipelines, a Novel nondestructive Testing (NDT) methodology using ultra-long (250 mm) Polymer Optical Fiber (POF) sensors coated with the Fe-C alloy film is proposed in this study. The theoretical principle is investigated to clarify the monitoring mechanism of this method, and the detailed fabrication process of this novel POF sensor is presented. To validate the feasibility of this novel POF sensor, exploratory research of the proposed method was performed using simulated corrosion tests. For simplicity, the geometric shape of the buried pipeline was simulated as a round hot-rolled plain steel bar. A thin nickel layer was applied as the inner plated layer, and the Fe-C alloy film was coated using an electroless plating technique to precisely control the thickness of the alloy film. In the end, systematic sensitivity analysis on corrosion severity was further performed with experimental studies on three sensors fabricated with different metal layer thicknesses of 25 μm, 30 μm and 35 μm. The experimental observation demonstrated that the sensor coated with 25 μm Fe-C alloy film presented the highest effectiveness with the corrosion sensitivity of 0.3364 mV/g at $\Delta m = 9.32 \times 10^{-4}$ g in Stage I and 0.0121 mV/g in Stage III. The research findings indicate that the detection accuracy of the novel POF sensor proposed in this study is satisfying. Moreover, the simple fabrication of the high-sensitivity sensor makes it cost-effective and suitable for the on-site corrosion monitoring of buried metal pipelines.

Keywords: polymer optical fiber; early-age corrosion monitoring; Fe-C alloy film; buried metal pipelines; acceleration corrosion

1. Introduction

1.1 Needs and necessity of corrosion monitoring of buried metal pipelines

In recent years, the construction scale of ultra-high Direct Current (DC) transmission networks have dramatically increased to satisfy the sustained growth in demand for electronic power. Meanwhile, long-distance buried metal pipelines have been built to transport oils and gases (Zeng *et al*. 2019, Yang *et al*. 2019, Chen *et al*. 2018). Due to the similar site selection requirements between the transmission networks of electronic power and oils or gases, intersecting and overlapping occurs during the transmission path, which will inevitably be affected by the DC transmission systems (Wang *et al*. 2013, Peng *et al*. 2019). As the DC grounding electrodes usually works in mono-polar mode and is regularly electro-discharged with a certain value, there will be some current flowing into the buried metal pipelines, resulting in the potential damage of the anti-corrosion layers and the electrochemical corrosion of metal pipeline networks (Feng *et al*. 2011). In extreme cases, the stray current will accelerate the corrosion perforation and leads to the rapid breakage of pipelines. Hence, the direct current interference on buried pipelines corrosion become severer and has received much research attention in the past few years (Guo *et al*. 2015, Zhu *et al*. 2014). However, the standards and design guidelines for determining the spatial distance between the buried metal pipelines and the DC grounding electrode have not been issued until now. In addition, the specific value and scientific time interval of electro-discharging, as well as other critical parameters, are still under-investigated. The early-age and in-situ monitoring on the corrosion of buried metal pipelines is of great significance to ensure the structural safety of transmission networks, predict the long-term remnant service life of pipelines, and provide warning of its possible failure risks.

1.2 Current corrosion monitoring techniques

To achieve the corrosion mechanism of the interference of DC current on the corrosion of the buried metal pipeline,

*Corresponding author, Ph.D.,
E-mail: chbchb@mail.tsinghua.edu.cn
[a] Associate Professor, E-mail: luodong@xjtu.edu.cn
[b] Student, E-mail: loo194108@stu.xjtu.edu.cn
[c] Professor, E-mail: yanghz@nwu.edu.cn
[d] Assistant Professor, E-mail: h.sun@northeastern.edu

ISSN: 1738-1584 (Print), 1738-1991 (Online)

various inspection tools and electrochemical corrosion sensors for monitoring pipeline corrosion processes have been developed. In general, pipeline inspection methods are designed to assess the health condition of a pipeline at a specific time instant and provide intuitive snapshots of the pipeline corrosion, such as potential survey technique (Kowalski 2014), IR coupons (Stears *et al.* 1997), magnetic flux leakages (Bai *et al.* 2014, Stawicki *et al.* 2010), ultrasonic transducers (Barbian *et al.* 2012), electro-magnetic acoustic transducers (Tiratsoo *et al.* 2013), eddy currents (Tiratsoo 2013) and external corrosion direct assessments (NACE 2002). However, these approaches are commonly limited by the high costs induced by the labor-intensive tasks, the highly specialized equipment and tremendous economic loss by service interruptions. Unlike conventional inspection methods, corrosion monitoring techniques using specially designed sensors, aim to identify the occurrence and the pattern of corrosion, as well as the corresponding deterioration rate. Many electrochemical techniques are generally capable of providing information regarding instantaneous corrosion rates (Beck *et al.* 2017), including linear polarization resistance (Stern *et al.* 1957), electrochemical impedance spectroscopy (Jankowski 2002), galvanic probes (Choi *et al.* 2007), multi-electrode arrays (Yang *et al.* 2002) and other single electrode methods (Barbalat *et al.* 2013). However, the presence of impressed current Cathodic Protection (CP) systems, the highly resistive soil environment and coated surfaces make the accurate in-situ measurements extremely challenging. Therefore, the existing corrosion monitoring techniques are not suitable for practical corrosion monitoring on buried metal pipelines.

1.3 Corrosion monitoring using conventional fiber optic sensors

In contrast, the advanced non-electrochemical methods (Du *et al.* 2016, Ren *et al.* 2017) mainly compare the metal losses at different time instants or indirectly evaluate the corrosion possibility through measuring physical variables utilizing Electrical Resistance (ER) probes (Li *et al.* 2017a, b) and optical fiber sensors (Zou *et al.* 2008, Yan *et al.* 2010). These corrosion detection methods are beneficial to understand the corrosion process and acquire the corrosion rates, and can also provide valuable information for optimizing the strategy to corrosion prevention. Recently, Fiber Optic Sensor (FOS) has achieved great leaps in the field of corrosion detection owing to its distinct characteristics including high sensitivity and detection accuracy, lightweight, long-distance monitoring capability, compactness, multiplexing performance and immunity to electromagnetic interference (Li *et al.* 2016, 2017a, b, Abdel-Jaber *et al.* 2019). One of the most widely used FOSs in Structural Health Monitoring (SHM) is Fiber Bragg grating (FBG) (Kinet *et al.* 2014, Ren *et al.* 2014, Hou *et al.* 2014), which has been successfully applied in detecting environmental corrosion (Islam *et al.* 2015, Al Handawi *et al.* 2016, Li *et al.* 2017a, b, Hou *et al.* 2013). In addition, Brillouin optical time-domain reflectometer is another popular technique to develop the corrosion sensor based on the propagation analysis of incident pulse train and Brillouin backscattering (Sun *et al.* 2014, Ren *et al.* 2018).

The active corrosion detection using fiber optic sensors plated by Fe-C alloy has been continuously improved to enhance the detection accuracy of steel corrosion with a more intelligent SHM system and methodology. It has been reported that the Long Period Gratings (LPGs) coated with Fe-C alloy films can detect the early stages of steel corrosion by observing the transmitted spectra (Chen *et al.* 2016, Tang *et al.* 2018). LPGs sensor usually consists of coating steel with a silver layer and Fe-C alloy film. The service life and corrosion possibility can be predicted according to thickness variation of the silver layer and Fe-C alloy film measured with LPGs sensors (Chen *et al.* 2017). Dong *et al.* (2006) proposed a nondestructive testing technique using the corrosion sensor composed of cladding etched multimode glass fiber plated by metal material. The corrosion process was inspected by observing the varying tendency of the output power. The scientific contribution of collected literature formed an important base and solid foundation for further developing techniques in the field of optical fiber corrosion sensors using sensitive films.

However, the aforementioned LPGs and non-cladded glass fibers present typical and apparent drawbacks, such as fragile material property and single-mode in transferring the corrosion information. Consequently, these kinds of sensors should be properly packaged in practical applications for overcoming their disadvantages. Comparatively, the solutions provided by Polymer Optical Fibers (POFs) are much more attractive because of the technological superiorities, including convenience in connecting operation, low cost, flexibility and large diameter. POF sensor is frequently employed in SHM and NDT testing due to its multiple functions in sensing displacement (Yang *et al.* 2014), vibration (Luo *et al.* 2016), strain, crack (Kuang *et al.* 2002, Luo *et al.* 2016) and liquid refractive index (Yang *et al.* 2014, 2015). Therefore, POF sensors can provide the necessary information with regard to various target objectives (Kuang *et al.* 2009). Moreover, the technical superiority and advantage of POF sensors will simplify the fabrication of POF sensors and offer bright commercial prospects, in particular for practical engineering applications. As an embedded sensor for monitoring the corrosion damage of buried metal pipelines, POF sensors with large core sizes usually present high resistance to fracture and corrosion, which will extend the service life of POF sensors and alleviate the additional cost of protection package superior to standard glass fibers from the perspective of high performance-price ratio.

In general, the preparation methods for metal film plating can be classified as magnetron sputtering, Physical Vapor Deposition (PVD) and electroless plating. The magnetron sputtering typically works in a high-temperature environment, which makes it easier to oxidize the Fe-C alloy. Meanwhile, the PVD process is time-consuming and very expensive. Furthermore, the thickness of Fe-C alloy film plated by the PVD fabrication process is not suitable for corrosion sensors due to the weak affinity between the loose-material Fe-C alloy film and the plastic surface. Furthermore, it is not feasible to prepare Fe-C alloy film

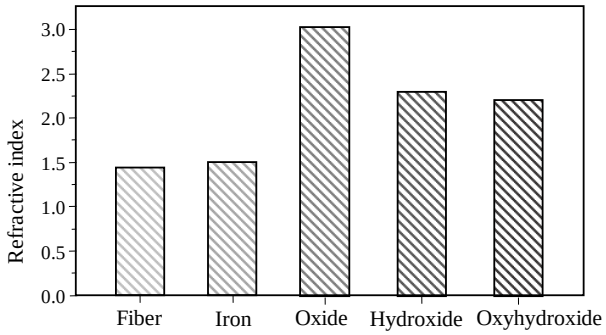

Fig. 1 Refractive index of optical fiber and iron rusts

directly by electroless plating, but this method can make the fiber surface metalized by plating a thin metal conductive film as a transition layer between the fiber core and Fe-C alloy film. Then, the electroplating technique can be employed to fabricate Fe-C alloy film. Therefore, the scientific preparation process composed of six key steps should be proposed to control the thickness of the Fe-C alloy film to form the required layer plating on the core of POF.

In order to overcome the drawbacks of existing corrosion monitoring method using POF sensors and improve the detection accuracy of corrosion defects in buried metal pipelines, a novel NDT testing methodology using ultra-long (250 mm) POF sensor coated with the Fe-C alloy film was proposed in this study. The proposed sensors were composed of nickel layer and outer film of Fe-C on the fiber. To clearly present the detection mechanism of this novel sensing technology, the sensing principles and theoretical analysis of the POF sensor were discussed in depth. To simplify the calibration process of electroplating Fe-C alloy film deposition, the inner nickel film, which works as the conductive film, was prepared by electroless deposition. Three sensors fabricated with different metal layer thicknesses of 25 μm, 30 μm and 35 μm were tested to investigate the influence of the Fe-C film thicknesses. The developed sensors were applied to monitor the corrosion test accelerated by the impressed current technique on buried metal pipelines simulated with round hot-rolled plain steel bars. The relationship between the change in the output voltages and the corrosion-induced mass loss of rebar during the corrosion process was established. The research findings indicate that the developed sensors are sensitive to the corrosion process and the corrosion severity of tested specimens can be precisely assessed. The experimental outcomes of the exploratory research present in this study can provide referential guidance on the practical engineering applications of the proposed corrosion sensing technology.

2. Theoretical sensing principles

2.1 Operational theory

The Fe-C alloy film has been extensively applied in the corrosion monitoring of metal structures to selectively replace part of the fiber coating by metal cladding. Fe-C metal alloy cover can efficiently absorb and reflect the light, and it can be treated as new waveguides for transmitting light to the photodetector. Fe-C alloy film begins to corrode due to chemical or electrochemical responses while the developed sensors are exposed in the corrosive environment. As the forefront defense layer, the passive film formed in the alkaline environment will be corroded first by chlorides attack. And then, the corrosion initiates from the outer surface of Fe-C alloy film, and the increasing accumulation of corrosion products constantly deteriorate the effective refractive index of the surrounding medium of developed sensors. In general, the typical rusts of iron are the mixture of oxides (FeO, Fe_2O_3, Fe_3O_4), hydroxides ($Fe(OH)_2$, $Fe(OH)_3$) and oxyhydroxides (α-FeOOH, β-FeOOH, γ-FeOOH, δ-FeOOH). The corresponding refractive indices are higher than that of iron and optical fiber, as presented in Fig. 1 (Refait *et al.* 2003). Finally, the corrosion product bonded on the sensor results in further expansion and damage, such as delamination, thinning and even desquamation to the Fe-C alloy film. The corroded metal plating disappears and will be entirely replaced by external media, including air, water and corrosive medium while complete corrosion of Fe-C alloy film occurs. In addition, the refractive indices of complex corrosion boundaries are lower than that of the fiber core. Consequently, the total reflection condition will amplify the output optical power. In the end, corrosion monitoring can be achieved by measuring the output light energy of the proposed sensor.

2.2 Sensor design

As exhibited in Fig. 2, the covered Fe-C alloy film acts as a metal-clad waveguide. In the metal-clad waveguide, the light-tracing model is employed to determine the wave path. The light path in the metal-cladded fiber sensor is illustrated in Fig. 2. The n_0, n_1, n_2 and n_3 refer to the refractive indices of the fiber core, coating and Fe-C alloy and external media, respectively. The beam is incident with an angle α_0 into the fiber and then propagates along the taper length L_0. The core height decreases from r_0 to r, where r_0 and r are the fiber core radius before and after polishing operation.

The tunneling light power $p_{tr}(z)$ directly affects the energy of Evanescent Waves (EWs), which can be described as Eq. (1) at the distance z (Luo *et al.* 2013).

$$p_{tr}(z) = \int_0^{n_2} d\bar{\beta} \int_{\sqrt{n_2^2-\bar{\beta}^2}}^{\sqrt{n_0^2-\bar{\beta}^2}} F(\bar{\beta},\bar{l})\exp -\gamma_{tr}(\bar{\beta},\bar{l})z d\bar{l} \quad (1)$$

where

$$\bar{b} = \frac{1}{r}\sqrt{n_0^2 r^2 - r_0^2 sin^2 a_0} \quad (2)$$

$$\bar{l} = \frac{1}{r} \times \sqrt{r_0^2 sin^2\alpha_0 - \left[n_0 r sin\left(\sin^{-1}\left(\frac{r_0 sin\alpha_0}{n_0 r}\right) - \tan^{-1}\left(\frac{2r_0(1-r)/r_0}{L_0}\right)\right)\right]^2} \quad (3)$$

As mentioned in Section 2.1, the lightwaves absorption

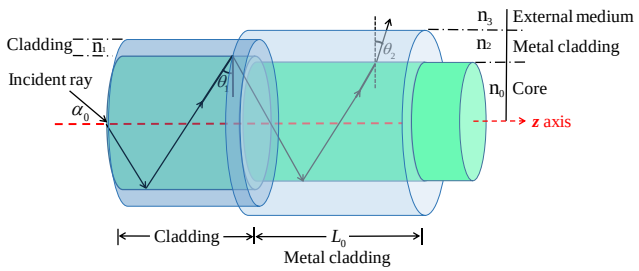

Fig. 2 Schematic of light propagation inside metal cladding

and reflection seriously depend on the metal plating. When light incident from the core to the metal surface, part of it will be reflected. However, the refracted lightwave is completely absorbed by the metal layer in a refraction angle of θ_2. Fig. 2 shows that θ_1 is the light angle incident between the fiber core and the plating interface. The lightwave transmission for the metal layer can be evaluated by the Fresnel formula T as expressed in Eq. (4)

$$T = \frac{n_2 \cos\theta_2}{n_0 \cos\theta_1}\left|\frac{2n_0 \cos\theta_1}{n_0 \cos\theta_1 + n_2 \cos\theta_2}\right|^2 \quad (4)$$

where n_2 is the refractive index of metal and it can be described as $n_2 = n_c(1 + ik)$. For Fe, n_c is set to 2.89 at the wavelength of 653 nm. k equals to $e^{-\alpha l}$ and it stands for the extinction coefficient that is usually adopted to represent the strong absorption of metal to lightwaves (Ordal *et al.* 1983). α is the absorption coefficient, which is related to the thickness of the metal layer l (Balberg *et al.* 1978). From the Fresnel formula, θ_2 can be obtained using Eqs. (5)-(6).

$$\cos\theta_2 = \left|\sqrt{1 - \left(\frac{n_1 \sin\theta_1}{n_2}\right)^2}\right| \quad (5)$$

$$\theta_1 = \frac{\pi}{2} - \sin^{-1}\left(\frac{\sin\alpha_0}{n_0}\right) \quad (6)$$

where θ_1 is the reflection angle (Refait *et al.* 2003).

In this study, the diameter of POF sensor employed was 1.0 mm. The refractive indexes of fiber core and cladding were 1.492 and 1.402, respectively. The numerical simulation was performed on the platform of Matlab. The Light-Emitting Diode (LED) with a wavelength of 660 nm was selected as the light source for numerical simulation. In order to excite the leaky light and generate more EWs, the incident light launch angle was obtained by polishing the facet of POF. The simulation result summarized in Fig. 3 indicates that the tunneling light power linearly increases with the incident radian angle of light source ranging from 0.01 (-0.01) rad to 0.05 (-0.05) rad. When θ_2 is within the range of -0.01 rad to 0.01 rad, the incident light is totally driven by the fiber, which is named as bond beam. Moreover, a greater refraction angle increases the tunneling light energy and its peak value occurs when θ_2 is equal to 1.0 rad. Since the refractive angle greatly depends on the absorption coefficient α and the metal layer thickness l, the metal layer thickness should be optimized to achieve the

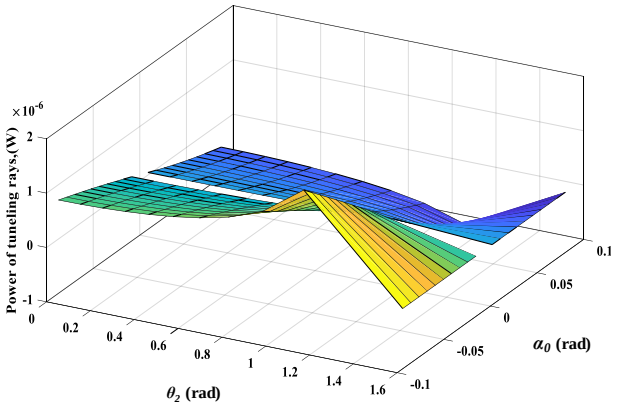

Fig. 3 Relationship between tunneling light power, incident light angle α_0 and refraction angle θ_2

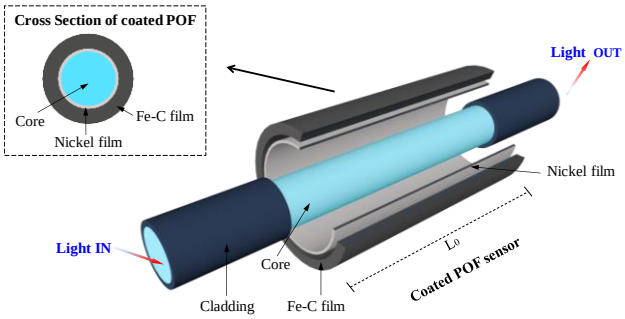

Fig. 4 Schematic of Fe-C alloy film-coated POF corrosion sensor

Fig. 3, the light tunneling power decreases from 1.51 ×10^{-6} W to 0.82 × 10^{-6} W while the θ_2 gradually drops from 1.0 rad to 0.01 rad. The research findings indicate that the tunneling light with the specific power of 0.69 × 10^{-6} W becomes the EWs, which means that the sensor reaches the most superior sensing performance. Therefore, more EWs can be observed when the incident light is lit with greater α_0 in sensors plated with thicker metal coating layers. As shown in Fig. 3, the highest tunneling light power can be reached where α_0 and θ_2 are -0.05 rad and 1.0 rad, respectively.

3. Fabrication processes of ultra-long polymer optical fiber-based corrosion sensor

As mentioned above, Fe-C alloy film cannot be directly coated on the fiber core surface using electroless plating process. In this study, a layer of metal palladium on POF was deposited and then a thin layer of metal nickel was electroless plated, for the purpose of enhancing the surface conductive of optical fibers. After these two essential steps, Fe-C alloy film can be plated by the electroplating technique. Additionally, scientific strategies for real-time monitoring on current density during the electroplating process and plating time duration are necessary to guarantee the required film thickness for Fe-C alloy.

The schematic of the Fe-C alloy film-coated POF corrosion sensor is shown in Fig. 4. Compared to other

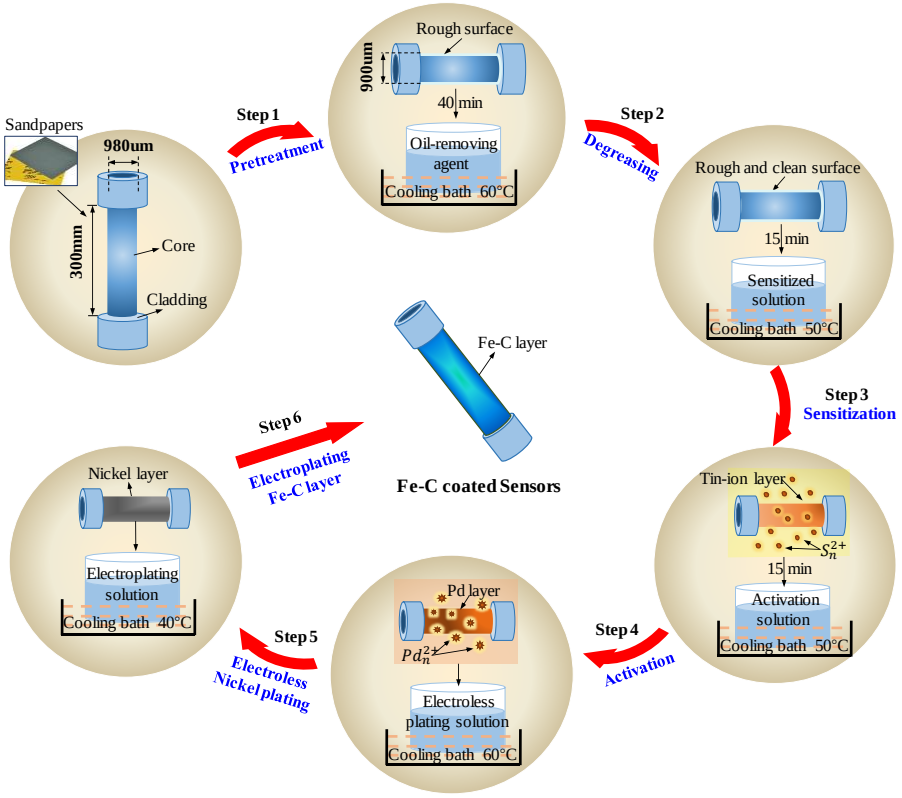

Fig. 5 Schematic diagram of fabrication processes for proposed sensor

preparation methods of PVD and magnetron sputtering, the combined method of electroless plating nickel film and electroplating Fe-C alloy film is a promising approach for achieving the mass production process at low cost due to its superiority of cost-effective equipment, low-temperature operating environment, multiple samples at a time in a larger operation space. As illustrated in Fig. 5, the fabrication process of the proposed sensor includes six key steps, which will be described in detail in the following sections.

3.1 Pretreatment

During the pretreatment process in this section, the Mitsubishi POFs with a diameter of 1.0 mm were utilized for exploratory research on ultra-long polymer optical fiber-based corrosion monitoring for buried metal pipelines. A fiber stripper was used to remove part of POF protective coat with a length of 250 mm. The raw sandpaper with 240-grit was employed for the elaborate removal of the fiber plating and portion of the core surface through grinding the fiber during rotation. The 960-grit sandpaper was then used to guarantee that multiple lines and micropores on the core surface can be evenly burnished and shaped until the fiber diameter reduced to 0.9 mm. During the grinding process, the white powders accumulated on the core surface were cleaned by cotton buds with the deionized water. The polishing operation can increase the roughness of the fiber surface, which is beneficial to improve the adhesion status between the fiber core and the metal layer. During the polishing process, the output light power was constantly monitored to guarantee the same output power of tapered fibers and identical tapered structure.

3.2 Degreasing

The hydrophobicity of the POF surface makes it difficult to conduct a chemical treatment using the aqueous solution as the carrier on the fiber surface. The degreasing process was used to get rid of oil spots on the POF surface. This is a basic operation that enhances adhesion between the coating film and the fiber core. In this section, the degreasing process was carried out with the oil removing agent named HT-601 (HANTE in China), which contained sodium hydroxide, trisodium phosphate, diethylene glycol diethanol mine and diethanol mine. The reagent was preheated to 60°C and completely stirred for 40 minutes before the fiber was processed. Through a wooden frame with alligator clips, two ends of the fiber were fastened to maintain the fiber upright. After degreasing, distilled water with a large flow was used to cautiously flush the fiber, for avoiding sensitization pollution led by degreasing liquids.

3.3 Sensitization

The sensitization and activation processes were designed to stimulate the catalytically active of fiber for the electroless cladding of the middle metal layer. A thin catalytic coating consisting of a reductive material (Sn^{2+}) was deposited on the bare fiber after degreasing. The sensitization tool utilized in this study was Act PP-950, manufactured by Ensoo chemical companies. The solution

was blended by 4 ml/L Act PP-950 and 270 ml/L (37%) analytical pure hydrochloric acid mixed with the deionized water. It should be noted that the hydrochloric acid component is not sulfuric. Under the temperature of 50°C, it took around 15 minutes for the sensitization process till a dark brown metal layer was formed on the surface of the fiber core.

3.4 Activation

The activation solution was JS Accelerate 960 produced by Ensoo. A total of 100 ml/L activation solution and deionized water were mixed together at 50°C for 15 minutes. The activation process aims to reduce the palladium ions (P_d^{2+}) using tin ions (S_n^{2+}) deposited on the core, according to the standard electrode potential of the palladium ($\phi'_{P_d^{2+}/P_d}$= 0.987 V) and the tin ($\phi'_{S_n^{4+}/S_n^{2+}}$= 0.15 V) as shown in Eq. (7).

$$S_n^{2+} + P_d^{2+} = P_d^0 + S_n^{4+} \tag{7}$$

Basically, the noble metal crystal nucleus, P_d^0, will be adsorbed by the fiber surface after the activation process, which can ensure the electroless plating of nickel to function effectively and helps to obtain a better adhesion between the nickel and the fiber surface. During the whole fabrication process, keeping the fiber straight is essential to guarantee the uniform coat of the palladium film. After the sensitization and activation process, the fiber was washed by deionized water with a small flow to avoid flushing away the palladium attached to the surface of optical fiber.

3.5 Electroless process of nickel film

The typical method for the electroless process of nickel film on the polymer surfaces is the alkaline electroless with sodium hypophosphite as a reduction agent. In this study, the electroless plating solution, the HT-801 was comprised of a potassium-phosphate, EDTA-2Na, ammonium-citrate, nickel sulfate and citric-acid, nickel sulfamic acid, and sodium hypophosphites. This solution was stirred at room temperature for 5 minutes before being used.

To avoid the deformation of the optical fiber due to the low working temperature of the proposed POF sensors, the alkaline solution was warmed using the cooling bath at 40°C. Only if the fiber stays straight throughout the electroplating process, a smooth and unitary nickel layer can be deposited. In addition, the thickness of nickel coating layer is controlled by the cladding time duration. Here, the deposition rate was about 25 μm/h. Therefore, it took about 100 s to deposit nickel layer on POF with a thickness of 650 nm. After completing the electroless plating operation, the samples were cleaned with distilled water and dried with a blower to ensure the surface of optical fibers is clean and free of chemical residues.

3.6 Electroplating Fe-C alloy film

After electroless process of nickel film detailed in Section 3.5, the Fe-C alloy film was electroplated on the surface of nickel layer. The electroplating solution constituted with 50 g/L $FeC_{l2} \cdot 4H_2O$, 1 g/L L-Ascorbic, 1.5 g/L Citrazinic acid, 0.5 g/L $C_{12}H_{35}NaO_4S$ and 3 g/L Saccharin sodium and has a pH of 3.2 at 40°C. It should be mentioned that before electroplating, the electrolysis cell must be energized to uniformly distribute the ions into the solution, which is a necessary procedure to guarantee that the uniform Fe-C alloy film can be deposited on the surface of POF. The ferrous solution of chloride includes citric acid and ascorbic acid wherein the reaction occurs, as described in Eq. (8).

$$Fe^{2+} + organic\ acid + 2e^- = Fe(C) \tag{8}$$

During the electroplating process, the optical fiber was connected via a power supply to the cathode under a constant current of 0.5 A/dm^2, and the anode of the electricity supply to the 20 # carbon steel. For acquiring effective adhesion between these two metals and uniform Fe-C alloy film, lower electroplating current density was implemented to the reaction process. The electroplating process lasted for 4.0 h, 4.8 h and 5.6 h to produce Fe-C alloy films with a thickness of 25 μm, 30 μm and 35 μm, respectively. For protecting the iron from corrosion, the coated fibers need to be rapidly immersed into NaOH solution to form a passive film, after the film deposition of Fe-C alloy.

4. Experimental investigation

Conceptually, in order to simulate the corrosion rate of metal pipelines, the proposed sensor and the tested objective have to be immersed in the same corrosive environment and spatial location. In this study, the special location of the proposed sensor was almost identical to that of the tested objective. In addition, the tested specimen and proposed sensors were immersed in the same corrosive solution. The relationship of corrosion severity between the proposed sensor and metal pipelines can be explicitly established.

4.1 Characterization analysis

To better understand the coating procedures, the microstructures in the main steps were pictured by a Scanning Electron Microscope (SEM, SU3500) coupled with an Energy Dispersive Spectroscopy (EDS). The 5.0 mm-long specimens were cut from additional fibers in different preparation stages and examined using SEM. The chemical compositions of nickel film and Fe-C alloy film were determined using EDS analysis. Additionally, the surface morphologies of corroded sensors which have immersed in 3.5 wt% NaCl solution for 24 hours were examined by SEM and EDS, for further verifying the variation of coating composition before and after corrosion.

4.2 Experimental setup of accelerated corrosion test

The photograph of the calibrated 250 mm length sensor

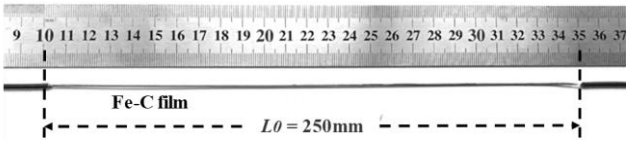

(a) Length of Fe-C alloy film-coated POF corrosion sensor

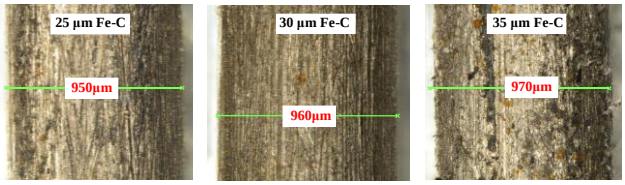

(b) Diameter of POF corrosion sensors coated with different Fe-C alloy films

Fig. 6 Photograph of Fe-C alloy film-coated POF corrosion sensor

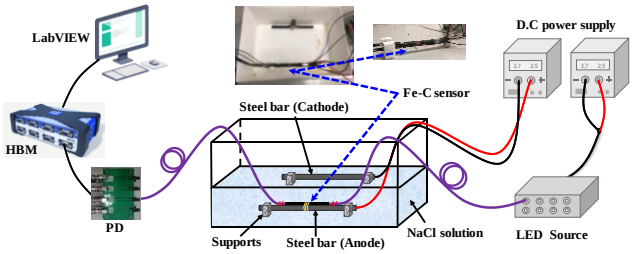

Fig. 7 Schematic of corrosion test using Fe-C alloy film-coated POF sensor

is shown in Fig. 6(a). Meanwhile, Fig. 6(b) shows the diameter of proposed sensors plated with three Fe-C alloy film thickness of 25 μm, 30 μm and 35 μm, using a superfield stereomicroscope (SMZ25).

As displayed in Fig. 7, the corrosion behavior was mimicked by immersing the proposed sensor into NaCl solution with concentrations of 3.5 wt% under the condition of the constant temperature of 25°C, which was the mixture of analytical grade NaCl and deionized water for simulating marine environment. The whole experimental configuration consisted of the accelerated corrosion device and the polymer optical fiber sensing system, as presented in Fig. 7. In this experiment, the impressed current technique was employed to accelerate the corrosion process of Fe-C alloy film-coated fiber. For simplicity, the metal pipeline herein was simulated using a steel bar with a diameter of 10 mm and a length of 350 mm. The steel bar wrapped with the proposed sensor using copper wire as the conductor was linked to the positive terminal of the DC power supply which provided the constant current of 1.0 A to simulate anode. Similarly, the other steel bar acting as a cathode was connected to the negative terminal of the DC power supply. The steady power in the fluid NaCl can be transferred from anode to cathode. As mentioned above, the electrical connection between the anodic rebar and sensor was achieved using copper wire.

To monitor the corrosion process, the polymer optical fiber sensing system was built, including a DC power supply, a Light-Emitting Diode (LED), polymer optical fiber sensors, a photodetector (PD) IF-D97, an HBM

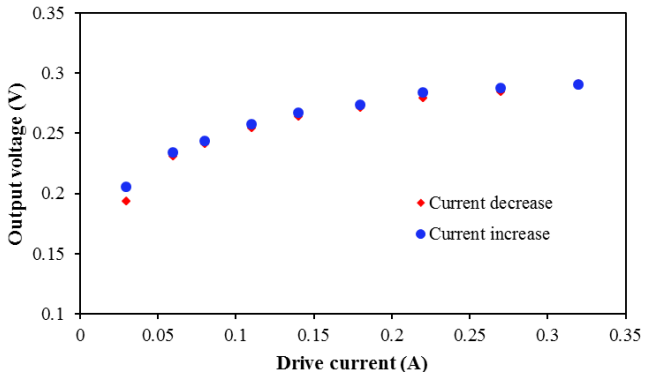

Fig. 8 Output voltage of proposed sensor drove by different current levels

Quantum X data acquisition device and a computer with LabVIEW program. The steady current was used for the LED with a wavelength of 660 nm to achieve excellent light energy stabilization. Two ends of the corrosion sensor were physically attached to the test objective (metal pipeline simulated by round hot-rolled plain steel bar) by the adhesive tape and connected to an LED. Besides, the other side was interposed to PD. The circuit was designed to detect the output of PD manufactured by Industrial Fiber Optics. The PD was linked to HBM equipped with a 24 bit A/D converter, which was used to receive light intensity and collect the voltage signals. A LabVIEW program was designed to collect the identified voltage and the sampling interval was set to 1.0 minute.

Fig. 8 shows the output voltage measured by the proposed sensor driven by the current at different levels, in order to verify the stability of proposed sensors. It can be clearly seen that the output voltage does not linearly increase with the drive current. However, the variation tendency of voltage value is stable, and the experimental observation corresponding to the increasing current process matches well with that of the decreasing current process.

5. Results and discussion

5.1 Characterization of nickel and Fe-C alloy film

The surface morphology plays a significant role in the working performance of optical fiber sensors. During the fabrication processes, the surface uniformity should be strictly controlled to guarantee the proportional relationship between the corrosion rate and the film thickness. The SEM images in Figs. 9(a)-(d) indicate that both the nickel film and Fe-C alloy film have been uniformly deposited through the well-controlled fabrication process detailed in Section 3. It can be seen from Figs. 9(c)-(d) that the sphere particles attached on the surface are composed of palladium, nickel and Fe-C cluster. The element composition of the nickel and Fe-C alloy film were further analyzed with EDX and the corresponding EDX patterns are summarized in Fig. 10. The nickel content in the deposited Ni layer reaches 68.21%, as illustrated in Fig. 10(a). Fig. 10(b) displays the EDX pattern of electroless deposited Fe-C alloy film with

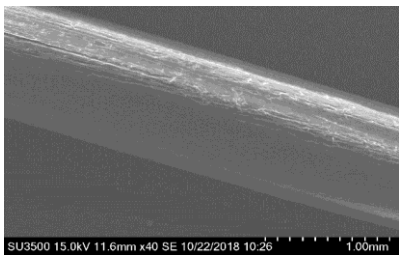

(a) Sensitization

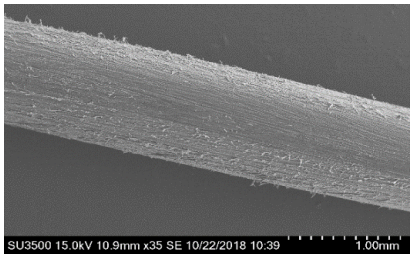

(b) Activation

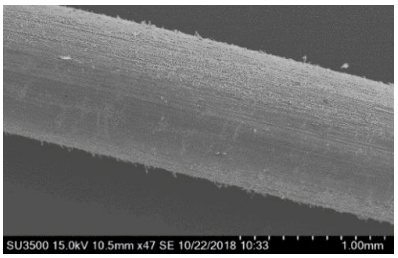

(c) Nickel film

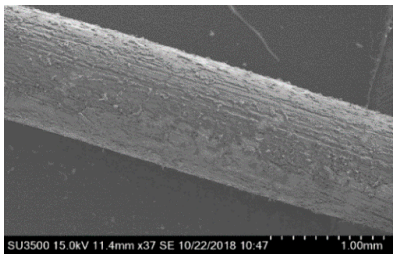

(d) Fe-C alloy film

Fig. 9 SEM images in different fabrication procedures

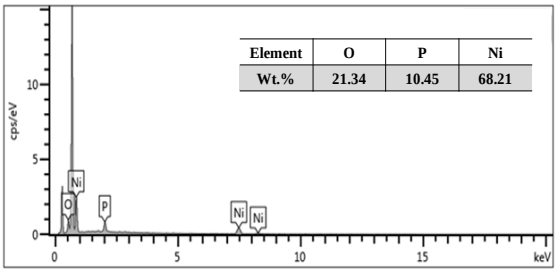

(a) Nickel film

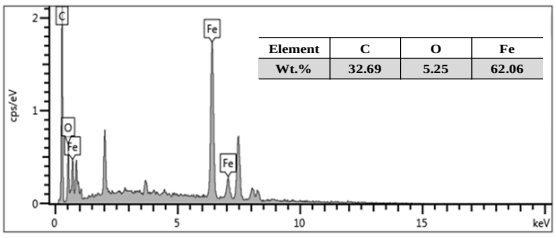

(b) Fe-C alloy film

Fig. 10 EDX patterns of Nickel layer and Fe-C alloy film

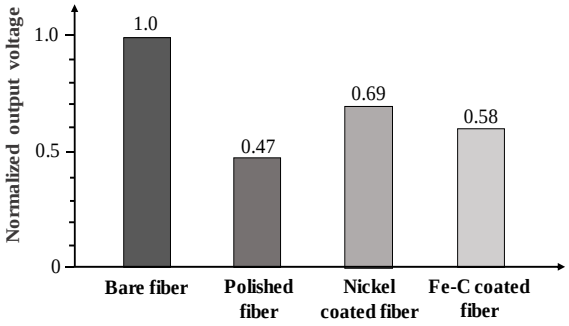

Fig. 11 Normalized output voltages of the proposed sensor during different fabrication procedures

the carbon content of 32.69 wt%, the oxygen content of 5.25 wt% and iron content of 62.06 wt%, respectively.

Fig. 11 shows that the normalized output voltages of the proposed sensor with a 25 μm Fe-C coated layer were not constant in different fabrication procedures, including bare fiber, pretreatment, nickel layer deposition and coating operation of Fe-C alloy film. The normalized output voltage of bare fiber reached the peak value while the convergence of lightwave propagating inside the fiber core occurred. Comparatively, the output voltage of polished POF with a diameter of 0.9 mm reduced to 0.47 and it increased to 0.69 after the coating process of the thin nickel layer. Due to the strong absorption of lightwaves by Fe-C metal cladding, the output voltage decreased to 0.58 after the deposition of the Fe-C alloy film.

5.2 Corrosion products

After corrosion testing lasted for 24 hours, the SEM photos of the corroded Fe-C layer and EDX pattern are shown in Figs. 12(a) and (b), respectively. The chloride ions in 3.5 wt% NaCl solution initiated the chemical corrosion of Fe-C alloy film after destroying the passivation film. The detailed chemical reaction can be expressed as follows

$$Fe \rightarrow Fe^{2+} + 2e^{-} \tag{9}$$

$$O_2 + 2H_2O + 4e^{-} \rightarrow 4OH^{-} \tag{10}$$

$$2Fe + O_2 + 2H_2O \rightarrow Fe(OH)_2 \tag{11}$$

In a corrosive environment, the chemical reaction is usually affected by oxygen content, resulting in complicated corrosion products. For instance, $Fe(OH)_2$ will be oxidized to $Fe(OH)_3$ and further dehydrates to Fe_2O_3. Without complete oxidization, $Fe(OH)_2$ will be reacted to Fe_3O_4 due to the insufficiency of oxygen. Both of these reactions will lead to a significant increase in oxygen content in corroded products.

Therefore, it can be concluded that oxygen concentration in Fig. 12(c) is higher than that of Fig. 10(b), which is 27.5 wt% and of 5.25 wt%, respectively. From SEM photos in Figs. 12(a)-(b), it can be clearly observed that the Fe-C alloy film has suffered serious corrosion since

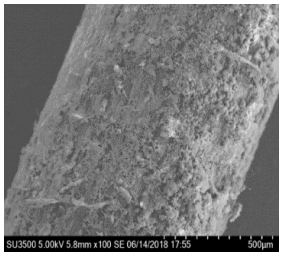

(a) Corroded fiber sensor

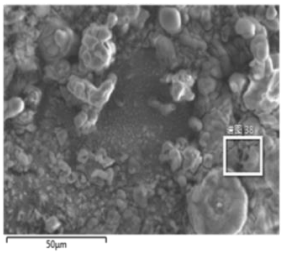

(b) Corroded Fe-C alloy film

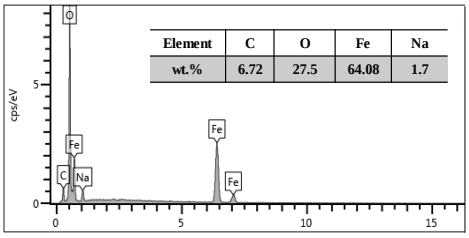

(c) EDX pattern

Fig. 12 SEM images and EDX pattern of corroded Fe-C alloy film

the surface has been completely covered with the thick layer consisted of corrosion products.

5.3 Voltage response of developed sensors

As indicated in Section 2.2, the output voltage of the proposed sensors depends on the effective refractive index of the environmental medium surrounding the fiber core and the metal film thickness, which changes with the corrosion activities of Fe-C alloy. In this study, the output voltages of all Fe-C plated POF sensors developed were collected using the PD, and the experimental data are summarized in Fig. 13(a). Before the beginning of the corrosion, the zero-setting for all sensors coated un-corroded Fe-C alloy layer with different thickness was needed. As illustrated in Fig. 13(a), a significant increase in the output voltage was observed for all types of sensors at the beginning of the immersion test. Then, the response of the output voltage kept stable and started decreasing gradually. Therefore, the varying trends of the output voltage measured from sensors coated by Fe-C alloy film with different thicknesses can be divided into three stages. The characteristics corresponding to each stage are discussed as follows.

5.3.1 Stage I - Increase

At the beginning of the corrosion test, the developed sensor was immersed in the NaCl solution. The outer passivation film acting as the protection of inner Fe-C alloy

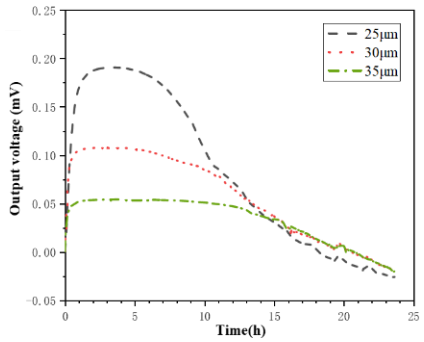

(a) Fe-C alloy film with three different thickness

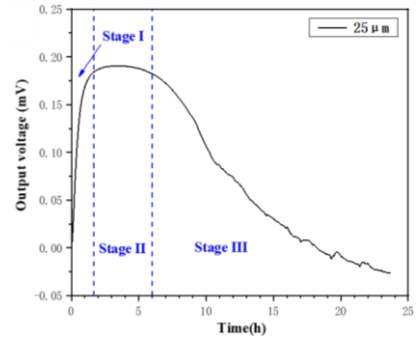

(b) Fe-C alloy film with 25 μm

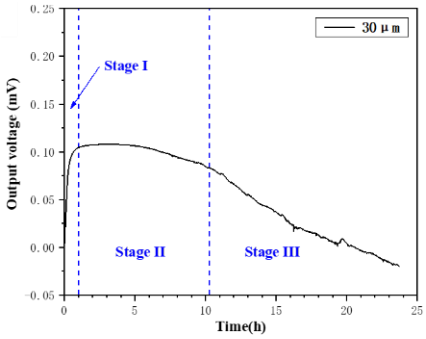

(c) Fe-C alloy film with 30 μm

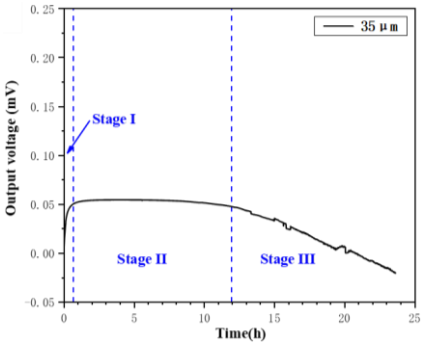

(d) Fe-C alloy film with 35μm

Fig. 13 Output voltages of sensors coated by Fe-C alloy film with different thicknesses

film from corrosion was rapidly attacked and eroded by a large number of chloride ions, resulting in damage and failure on the outer surfaces of sensors. Subsequently, the Fe-C alloy film was corroded by chloride, water ions and oxygen, and part of these corrosive substances infiltrated into the Fe-C alloy film through pores on the surface. The NaCl solution has replaced the pre-existing air in the fiber cladding and amplified the refractive index of the coating

surrounding the fiber. As a result, the output voltage increased accordingly.

Meanwhile, the Fe atoms started bonding with the oxygen atoms to form the hydration Fe-$(OH)_n$. Compared with the chemical bond strengths in Fe-Fe and Fe-C, the bond strength between Fe and $(OH)_n$ is the weakest. As the corrosion process continues, the hydroxyls or oxygen atoms invaded the deeper layers of Fe-C alloy film. Consequently, the effective thickness of Fe-C alloy film dropped sharply induced by rapid chemical reactions, as shown in Eqs. (9)-(11). The corrosion products started accumulating on the outer layer, and ulteriorly increased the refractive index of the surrounding medium, resulting in the increment of the output voltage, as discussed in Section 2.1. Therefore, the significant increase of the output voltage in Stage I was attributed to the change in the effective environmental refractive index due to the infiltration of the corrosive solution, reduction of Fe-C alloy film and generation of corrosion products.

5.3.2 Stage II - Stabilization

After the depassivation, the corrosion of Fe-C alloy film initiated and extended to deeper and larger regions due to the sufficient contact with corrosive substances. More Fe-C alloys were converted to the typical rusts at different oxidation levels, which consist of iron oxides, iron hydroxide, and iron oxyhydroxides. The expansion coefficients of all corrosion products are higher than that of iron itself. These newly generated corrosion products and un-corroded Fe-C alloy formed a thicker coating attached to the surface of fiber core at the beginning of Stage II, which led to less infiltration of corrosive substances and reduced the corrosion rate compared with these in Stage I. Therefore, the effective refractive index of the environment around the sensor remained almost constant in the meantime, thus maintaining the relatively stable output voltage. As time went on, rusts gradually peeled off from the surface of the developed sensors due to the further volume expansion of corrosion products and long-term immersion in corrosive solution, which resulted in a slight reduction in output voltage. In this stage, the enlargement of the corrosion area, Fe-C alloy film thinning or generation of corrosion products and desquamation of outer rust layer, all together affected the environmental refractive index surrounding the fiber.

5.3.3 Stage III - Decrease

Gradually, the Fe-C alloy film became thinner and eventually disappeared after being completely corroded. Meanwhile, the massive corroded layer covered the entire fiber separated from the fiber due to the volume expansion from iron to corrosion products. Therefore, the moderate decrease of the output voltage in Stage III is ascribed to weaken corrosion activities as well as desquamation of corrosion products.

After the immersion test of 24 hours, it can be clearly observed that the output voltage of 24 hours was significantly lower than that of the experiment beginning, as shown in Fig. 13. The experimental observation was consistent with the detailed corrosion process of the Fe-C alloy film discussed in Section 5.1. In this study, the polished fiber without any coated metal layer was also exposed to the NaCl solution for comparison. Moreover, the normalized output voltages of the proposed sensor coated the Fe-C alloy film was about 0.58, and that of polished POF reduced to 0.47 after the disappearance of metal film.

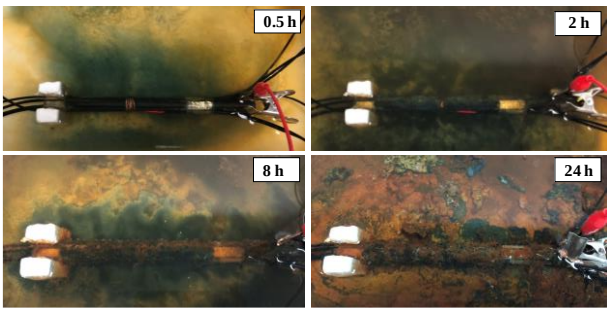

Fig. 14 States of the proposed sensors at the different stages in accelerate corrosion test

In Section 2.2, the theoretical relationship between tunneling light power, incident light angle α_0 and refraction angle θ_2 was simulated, as presented in Fig. 3. The simulation findings are beneficial for understanding the corrosion behaviors at the abovementioned three stages. The specific value of θ_2 is directly related to the thickness of the plated metal film and the generation of corrosion products. As detailed in Section 2.2, the tunneling light power increases with the refraction angle θ_2 and reaches the maximum value while θ_2 equals to 1.0 rad. And then, the tunneling light power linearly decreases when θ_2 ranges from 1.0 rad to 1.6 rad. With the constant incident light angle, the varying trends of tunneling light power at different refraction angles are basically consistent with that shown in Fig. 13. In Stage I, as the thickness of the Fe-C alloy film became smaller, the output voltage of the sensor increased accordingly. After reaching the peak value at the middle period of Stage II, the voltage constantly decreased with the continuation of the corrosion process until the end of Stage III.

Fig. 14 presents the states of the corrosion sensors and the variation of corrosive environmental color over time. It is obviously observed that the change in the NaCl solution color from clear at the beginning of test to the grey-green at 0.5 h, and this is because that the deficient oxidation results more ferrous hydroxide production, which needs to be further oxidized to ferric ion under the condition of adequate oxygen. Similarly, the color of corrosion products at 2.0 h in Stage I was grey-green, and part of solution was dark brown. At 8.0 h in Stage II, it is noticeable that massive red-brown rusts accumulated on the surface of the steel bar to form a thicker coating, which impedes the corrosion activities, as mentioned above. At the end of the corrosion test, the corrosion products have diffused and dissolved in the corrosion solution.

5.4 Influence of Fe-C alloy film thickness

As illustrated in Fig. 13(a), the variation tendencies of output voltages of sensors coated by Fe-C alloy film with

different thicknesses are similar, which means that the monitoring mechanism of developed sensors coated by Fe-C composite films with the thickness of 25 μm, 30 μm and 35 μm are basically the same. It is also noticeable that the thickness of Fe-C alloy film affects the termination time and the range of output voltage change for Stages I-III. In Figs. 13(b)-(d), the output voltage of POF corrosion sensors coated with 25 μm, 30 μm and 35 μm increased to 0.18 mV, 0.11 mV and 0.05 mV after approximately 1.7 h, 1.1 h and 0.8 h of immersion test in Stage I. The working performance of the sensor is the highest while the thickness of the Fe-C alloy film is 25 μm. In contrast, the relative variation in output voltage is lowest in the sensor where Fe-C alloy film is the thickest, namely 35 μm, which means that the sensitivity of the proposed sensors presents a negative correlation with the Fe-C alloy film. This is because the thinner Fe-C alloy film is more sensitive to the change in the environmental refractive index surrounding the fiber core. Meanwhile, more pores on the surface of the thinner Fe-C layer result in more penetration of corrosive solution and more aggressive corrosion activities.

In Stage II, the duration times of stabilization were 4.2 h, 9.2 h and 11.1 h for 25 μm, 30 μm and 35 μm Fe-C alloy film, respectively. The thinner thickness of Fe-C alloy film had a shorter stabilization time of output voltage. This is due to the fact that the corrosion sensors with Fe-C alloy film of 35 μm possess thicker corrosion product layer, which makes it difficult for the corrosive medium to penetrate into the intact Fe-C alloy and decrease the corrosion rates. Meanwhile, the desquamation of the outermost rust layer has little effect on the changes in the output voltage for the thicker Fe-C film.

In Stage III, the thickness of Fe-C alloy film affects the decrease rate of output voltage. The voltage signal of the 25 μm Fe-C film sensor drops much more shapely, compared with the other two sensors. Corrosion activities gradually slow down and even stop in Stage III. Consequently, the corrosion products covered on the fiber core played a dominant role in the environmental refractive index. Therefore, the sensors with the thinner Fe-C layer were more sensitive to the falling off of the thinner corrosion product layer. Additionally, it can be concluded that the fitting equation for the quantitative description of output voltage-time curves in Stage I and Stage III can be employed to assess the corrosion severity of tested objectives.

5.5 Relationship between sensor responses and corrosion-induced mass loss

According to the research findings in Section 5.4, the corrosion severity of tested objectives can be evaluated using the relationships between the corrosion-induced mass loss of tested rebar and voltage responses of Fe-C coated sensors established by the immersion test in which the monitoring targets and the proposed sensor are exposed to identical corrosive environments. In this study, the relationships of corrosion-induced mass loss of the steel and sensor's responses in Stage I and Stage III are fitted using second-order polynomial curves and linear equations respectively, as exhibited in Figs. 15(a)-(b).

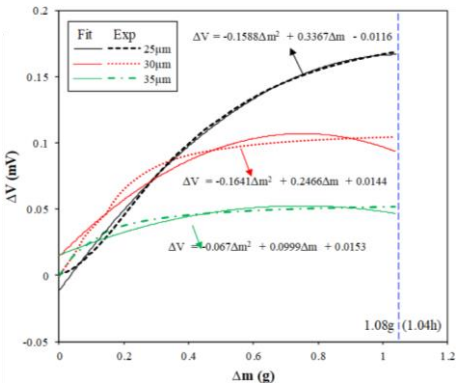

(a) Stage I

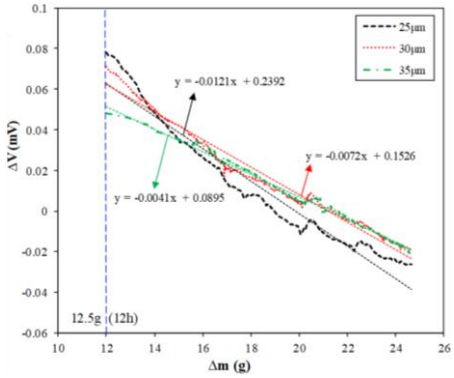

(b) Stage III

Fig. 15 Relationships between corrosion-induced mass loss of rebar and voltage responses of pro-posed sensors

Here, the Faraday Law is employed to calculate the mass loss of rebar according to the applied current and corrosion time, as shown in Eq. (12). And then, the second-order polynomial curve is used to fit the relationships of sensor responses and the mass losses.

$$\Delta m = \frac{MIt}{ZF} \tag{12}$$

where Δm is the mass of steel loss in g; I is the corrosion current in ampere; t indicates corrosion time in second; F is the Faraday's constant (96487 C/mol); Z is the number of electrons transferred (Fe = 2); M is the molar mass (Fe = 55.847 g/mol).

Throughout the corrosion process, the voltage in accelerated corrosion system was observed to have a minor fluctuation with the highest variation of 8 V. This is because that the generation of corrosion products and the thinning of Fe-C alloy have increased the resistance of the whole system.

As shown in Fig. 15(a), the fitting function is capable of depicting the Δm-ΔV curves and the correlation coefficients (R^2) are higher than 0.91. The sensitivity of proposed sensors can be defined as the slopes of fitted curves in Fig. 15. Accordingly, the sensor sensitivity can be denoted as 0.3364 mV/g (Δm = 9.32 × 10^{-4} g, 25 μm), 0.2465 mV/g (Δm = 8.275 × 10^{-5} g, 30 μm) and 0.0999 mV/g (Δm = 1.775 × 10^{-5} g, 35 μm), respectively. Therefore, the sensors coated by Fe-C alloy film with the thickness is the most sensitive

to the changing trend of corrosion level in Stage I, which is consistent with the basic conclusion drawn in Section 5.3.

Fig. 15(b) shows the sensitivities of proposed sensors during corrosion time from 5 hours to 24 hours. As marked in Fig. 15(b), all of the curves can be fitted using linear equations and the values of R^2 are higher than 0.91. At Stage III, the sensitivity coefficients herein are 0.0121 mV/g, 0.0072 mV/g and 0.0041 mV/g, respectively. In general, it can be seen that the sensor coated with a 25 μm Fe-C alloy film presents the highest sensitivities to the corrosion deterioration process in Stage I and Stage III. More specifically, the sensitivity coefficient corresponding to the film thickness of 25 μm is almost three times higher than that of the sensor coated with a 35 μm Fe-C alloy film.

In this study, the A/D conversion rate of the acquisition system is 24 bit s^{-1}. Therefore, the voltage resolution is about 0.298 μV while the reference voltage is set to 5 V. The sensor coated with a 25 μm Fe-C alloy film is able to capture the mass loss of rebar as small as 0.886 mg in Stage I and 24.6 mg in Stage III. Such a high corrosion detection sensitivity makes the proposed sensor suitable for in-situ detection of the mass loss for buried metal pipelines.

6. Conclusions

To improve the detection accuracy of corrosion defects in buried metal pipelines, a novel NDT testing methodology using the ultra-long (250 mm) POF sensor coated with the Fe-C alloy film was proposed in this study. The detection mechanism of this novel sensing technology, the sensing principles and theoretical analysis of the POF sensor were discussed in depth. Exploratory experiments were performed and the feasibility of the proposed corrosion monitoring was fully validated. Based on the theoretical and experimental research findings, the main conclusion of this study can be made as follows:

• The light-tracing model was employed to simulate the theoretical relationship between tunneling light power, incident light angle α_0 and refraction angle θ_2. The result indicated that the tunneling light energy first increased and then decreased with the increment of the refraction angle, and reached a peak value while θ_2 was equal to 1.0 rad. Since the thickness of the metal layer and the generation of corrosion products all together affect the refraction angle during the corrosion process, the research finding can help understand the corrosion sensing mechanism and optimize the sensor performance.

• Due to the special material properties of polymer optical fiber, the inner nickel films with the thickness of 650 nm as a transition layer were electroless plated firstly, and then the outer Fe-C alloy films with the thickness of 25 μm, 30 μm and 35 μm were fabricated by electroplating technique. The entire fabrication includes six key steps, in which the control of current density and electroplating time in the electroplating process is of great significance to obtain the required Fe-C films. The morphologies and components of the sensor surface were measured by SEM and EDX during the fabrication processes, and the influence of different fabrication procedures on the output voltages of the proposed sensor was analyzed.

• To test the sensor performance in a short experiment period, the accelerated corrosion method was designed by immersing the proposed sensor into 3.5 wt% NaCl solution. The experimental finding showed that the output voltage response of the proposed sensors with different Fe-C alloy film thickness changing over corrosion time was divided into three stages of significant increase, stabilization and slow decrease. Moreover, the thickness of Fe-C alloy film affected the termination time and the range of output voltage change in Stages I-III, and the 25 μm Fe-C film sensor was the most sensitive one with a sensitivity of 0.3364 mV/g (Δm = 9.32 × 10^{-4} g) in Stage I and 0.0121 mV/g in Stage III. Such a high corrosion detection sensitivity makes the proposed sensor suitable for in-situ corrosion monitoring for buried metal pipelines.

The detectability of the corrosion process of buried metal pipelines has been verified by the exploratory research on ultra-long polymer optical fiber-based corrosion sensing for buried metal pipelines performed in this study. The developed sensor presents distinct technical advantages, including low-cost, convenience in fabrication, high sensitivity. The experimental researches on the sensitivity of developed sensors in different corrosive environments and their practical application will be performed in the follow-up studies.

Acknowledgments

This research was supported by National Postdoctoral Science Foundation (No. 2019M650688), National Natural Science Foundation of China (No. 51908320), Central University's Special Research Fund Interdisciplinary Project (No. xjj2017175), Natural Science Foundation Research Program of Shaanxi Province-Youth Talents Project (2016JQ5017) and Research Fund Project of Xi'an Jiao Tong University (No. 1191320036).

References

Abdel-Jaber, H. and Branko, G. (2019), "Monitoring of long-term pre-stress losses in pre-stressed concrete structures using fiber optic sensors", *Struct. Health Monit.*, **18**(1), 254-269. https://doi.org/10.1177/1475921717751870.

Al Handawi, K., Vahdati, N. and Rostron, P. (2016), "Strain based FBG sensor for real-time corrosion rate monitoring in pre-stressed structures", *Sens. Actuators B Chem.*, **236**, 276-285. https://doi.org/10.1016/j.snb.2016.05.167.

Bai, Y. and Bai, Q. (2014), *Subsea Pipeline Integrity and Risk Management*, Gulf Professional Publishing, Oxford, UK.

Balberg, I. and Pinch, H.L. (1978), "The optical absorption of iron oxides", *J. Magn. Magn. Mater.*, **7**(1-4), 12-15. https://doi.org/10.1016/0304-8853(78)90138-5.

Barbalat, M., Caron, D., Lanarde, L., Meyer, M., Fontaine, S., Castillon, F., Vittonato, J. and Refait, P.H. (2013), "Estimation of residual corrosion rates of steel under cathodic protection in soils via voltammetry", *Corros. Sci.*, **73**, 222-229. https://doi.org/10.1016/j.corsci.2013.03.038.

Barbian, A. and Beller, M. (2012), "In-line inspection of high-pressure transmission pipelines: State-of-the-art and future trends", *Proceedings of the 18th World Conference on Nondestructive Testing*, Durban, South Africa, April.

Beck, J., Hall, D.M., Ziomek-Moroz, M. and Lvov, S.N. (2017), "Membrane-based electrochemical sensor for corrosion monitoring in natural gas pipelines", *ECS Trans.*, **77**(11), 681. https://doi.org/10.1149/07711.0681ecst.

Chen, Y., Tang, F. and Bao, Y. (2016), "A Fe-C coated long-period fiber grating sensor for corrosion-induced mass loss measurement", *Opt. Lett.*, **41**(10), 2306-2309. https://doi.org/10.1364/OL.41.002306.

Chen, Y., Tang, F. and Tang, Y. (2017), "Mechanism and sensitivity of Fe-C coated long period fiber grating sensors for steel corrosion monitoring of RC structures", *Corros. Sci.*, **127**, 70-81. https://doi.org/10.1016/j.corsci.2017.08.021.

Chen, B., Hei, C., Luo, M., Ho, M.S. and Song, G. (2018), "Pipeline two-dimensional impact location determaination using time of arrival with instant phase (TOAIP) with piezoceramic transducer array", *Smart Mater. Struct.*, **27**(10), 105003. https://doi.org/10.1088/1361-665X/aadaa9.

Choi, Y.S., Kim, J.G. and Koo, J.Y. (2007), "A galvanic sensor for monitoring the corrosion damage of buried pipelines: Part 3-correlation of probe current to cathodic protection and stray current", *Corrosion*, **63**(10), 951-957. https://doi.org/10.5006/1.3278313.

Dong, S., Liao, Y. and Tian, Q. (2006), "Optical and electrochemical measurements for optical fiber corrosion sensing techniques", *Corros. Sci.*, **48**(7), 1746-1756. https://doi.org/10.1016/j.corsci.2005.05.025.

Du, G., Kong, Q., Wu, F., Ruan, J. and Song, G. (2016), "An experimental feasibility study of pipeline corrosion pit detection using a piezoceramic time reversal mirror", *Smart Mater. Struct.*, **25**(3), 037002. https://doi.org/10.1088/0964-1726/25/3/037002.

Feng, X., Zuo, Y., Tang, Y., Zhao, X. and Lu, X. (2011), "The degradation of passive film on carbon steel in concrete pore solution under compressive and tensile stresses", *Electrochim. Acta.*, **58**, 258-263. https://doi.org/10.1016/j.electacta.2011.09.035.

Guo, Y.B., Liu, C., Wang, D.G. and Liu, S.H. (2015), "Effects of alternating current interference on corrosion of X60 pipeline steel", *Petrol. Sci.*, **12**(2), 316-324. https://doi.org/10.1007/s12182-015-0022-0.

Hou, Q., Ren, L., Jiao, W., Zou, P. and Song, G. (2013), "An improved negative pressure wave method for natural gas pipeline leak location using FBG based strain sensor and wavelet transform", *Math. Probl. Eng.*, **2013**, 278794. https://doi.org/10.1155/2013/278794.

Hou, Q., Jiao, W., Ren, L., Cao, H. and Song, G. (2014), "Experimental study of leakage detection of natural gas pipeline using FBG based strain sensor and least square support vector machine", *J. Loss Prevent. Proc.*, **32**, 144-151. https://doi.org/10.1016/j.jlp.2014.08.003.

Islam, M.R., Bagherifaez, M. and Ali, M.M. (2015), "Tilted fiber bragg grating sensors for reinforcement corrosion measurement in marine concrete structure", *IEEE Trans. Instrum. Meas.*, **64**(12), 3510-3516. https://doi.org/10.1109/tim.2015.2459511.

Jankowski, J. (2002), "Electrochemical methods for corrosion rate determination under cathodic polarisation conditions: A review part I-DC methods", *Corros. Rev.*, **20**(3), 159-178. https://doi.org/10.1515/CORRREV.2002.20.3.159.

Kinet, D., Mégret, P., Goossen, K.W., Qiu, L., Heider, D. and Caucheteur, C. (2014), "Fiber bragg grating sensors toward structural health monitoring in composite materials: Challenges and solutions", *Sensors*, **14**(4), 7394-7419. https://doi.org/10.3390/s140407394.

Kowalski, A. (2014), *Underground Pipeline Corrosion*, Woodhead Publishing, Cambridge, UK.

Kuang, K.S.C., Cantwell, W.J. and Scully, P.J. (2002), "An evaluation of a novel plastic optical fiber sensor for axial strain and bend measurements", *Meas. Sci. Technol.*, **13**(10), 1523. https://doi.org/10.1088/0957-0233/13/10/303.

Kuang, K.S.C., Quek, S.T. and Maalej, M. (2009), "Plastic optical fiber sensor for structural health monitoring: A review of recent progress", *J. Sens.*, **2009**, 312053. https://doi.org/10.1155/2009/312053.

Li, S.Y., Jung, S.W., Park, K.W., Lee, S.M. and Kim, Y.G. (2007a), "Kinetic study on corrosion of steel in soil environments using electrical resistance sensor technique", *Mater. Chem. Phys.*, **103**(1), 9-13. https://doi.org/10.1016/j.matchemphys.2007.02.076.

Li, S.Y., Kim, Y.G., Jung, S.W., Song, H.S. and Lee, S.M. (2007b), "Application of steel thin film electrical resistance sensor for in situ corrosion monitoring", *Sens. Actuators B Chem.*, **120**(2), 368-377. https://doi.org/10.1016/j.snb.2006.02.029.

Li, W., Ho, S.C.M. and Song, G. (2016), "Corrosion detection of steel reinforced concrete using combined carbon fiber and fiber bragg grating active thermal probe", *Smart Mater. Struct.*, **25**(4), 045017. https://doi.org/10.1088/0964-1726/25/4/045017.

Li, W., Ho, S.C.M., Luo, M., Huynh, Q. and Song, G. (2017a), "Fiber optic macro-bend-based sensor for detection of metal loss", *Smart Mater. Struct.*, **26**(4), 045002. https://doi.org/10.1088/1361-665X/aa5d5d.

Li, W., Xu, C., Ho, S.C.M., Wang, B. and Song, G. (2017b), "Monitoring concrete deterioration due to reinforcement corrosion by integrating acoustic emission and FBG strain measurements", *Sensors*, **17**(3), 657. https://doi.org/10.3390/s17030657.

Luo, D., Ibrahim, Z. and Ma, J. (2016), "Tapered polymer fiber sensors for reinforced concrete beam vibration detection", *Sensors*, **16**(12), 2149-2163. https://doi.org/10.3390/s16122149.

Luo, D., Ibrahim, Z., Ismail, Z. and Xu, B. (2013), "Optimization of the geometries of biconical tapered fiber sensors for monitoring the early-age curing temperatures of concrete specimens", *Comput. Aided Civ. Inf.*, **28**(7), 531-541. https://doi.org/10.1111/mice.12022.

Luo, D., Yue, Y. and Li, P. (2016), "Concrete beam crack detection using tapered polymer optical fiber sensors", *Measurement*, **88**, 96-103. https://doi.org/10.1016/j.measurement.2016.03.028.

NACE, R.P. (2002), *Pipeline External Corrosion Direct Assessment Methodology*, NACE International, Houston, Texas, USA.

Ordal, M.A., Long, L.L., Bell, R.J., Bell, S.E., Bell, R.R., Alexander, R.W. and Ward, C.A. (1983), "Optical properties of the metals Al, Co, Cu, Au, Fe, Pb, Ni, Pd, Pt, Ag, Ti and W in the infrared and far infrared", *Appl. Opt.*, **22**(7), 1099-1119. https://doi.org/10.1364/AO.22.001099.

Peng, J.X., Xiao, L.F., Zhang, J.R., Cai, C.S. and Wang, L. (2019), "Flexural behavior of corroded HPS beams", *Eng. Struct.*, **195**, 274-287. https://doi.org/10.1016/j.engstruct.2019.06.006.

Refait, P., Memet, J.B. Bon, C., Sabot, R. and Génin, J.M.R. (2003), "Formation of the fe(II)-fe(III) hydroxysulphate green rust during marine corrosion of steel", *J. Corros. Sci.*, **45**(4), 833-845. https://doi.org/10.1016/S0010-938X(02)00184-1.

Ren, L., Jia, Z.G., Li, H.N. and Song, G. (2014), "Design and experimental study on FBG hoop-strain sensor in pipeline monitoring", *Opt. Fiber Technol.*, **20**(1), 15-23. https://doi.org/10.1016/j.yofte.2013.11.004.

Ren, L., Jiang, T., Li, D.S., Zhang, P., Li, H.N. and Song, G.B. (2017), "A method of pipeline corrosion detection based on hoop-strain monitoring technology", *Struct. Control Health*, **24**(6), 1931. https://doi.org/10.1002/stc.1931.

Ren, L., Jiang, T., Jia, Z.G., Li, D.S., Yuan, C.L. and Li, H.N. (2018), "Pipeline corrosion and leakage monitoring based on the distributed optical fiber sensing technology", *Measurement*, **122**, 57-65. https://doi.org/10.1016/j.measurement.2018.03.018.

Stears, C.D., Degerstedt, R.M., Moghissi, O.C. and Bone, L.III. (1997), "Field program on the use of coupons to monitor cathodic protection of an underground pipeline", *Proceedings of the 1997 Corrosion 97 NACE International*, New Orleans, Louisiana, USA, March.

Stern, M. and Geary, A.L. (1957), "Electrochemical polarization I. A theoretical analysis of the shape of polarization curves", *J. Electrochem. Soc.*, **104**(1), 56-63. https://doi.org/10.1149/1.2428472.

Sun, Y., Shi, B. and Chen, S.E. (2014), "Feasibility study on corrosion monitoring of a concrete column with central rebar using BOTDR", *Smart Struct. Syst., Int. J.*, **13**(1), 41-53. https://doi.org/10.12989/sss.2014.13.1.041.

Tang, F., Chen, Y. and Li, Z. (2018), "Application of Fe-C coated LPFG sensor for early stage corrosion monitoring of steel bar in RC structures", *Constr. Build. Mater.*, **175**, 14-25. https://doi.org/10.1016/j.conbuildmat.2018.04.187.

Thomas, B. and Bryce, B. (2010), "Monitoring of top of line corrosion with eddy current technology combined with magnetic flux leakage method", *Proceedings of the Corrosion 2010 NACE International*, San Antonio, Texas, USA, March.

Tiratsoo, J. (2013), *Pipeline Pigging and Integrity Technology*, Clarion Technical Publishers, Houston, Texas, USA.

Wang, L.W., Du, C.W., Liu, Z.X., Wang, X.H. and Li, X.G. (2013), "Influence of carbon on stress corrosion cracking of high strength pipeline steel", *Corros. Sci.*, **76**, 486-493. https://doi.org/10.1016/j.corsci.2013.06.051.

Yang, L., Sridhar, N., Pensado, O. and Dunn, D.S. (2002), "An in-situ galvanically coupled multielectrode array sensor for localized corrosion", *Corrosion*, **58**(12), 1004-1014. https://doi.org/10.5006/1.3280789.

Yan, S.Z. and Chyan, L.S. (2010), "Performance enhancement of BOTDR fiber optic sensor for oil and gas pipeline monitoring", *Opt. Fiber Technol.*, **16**(2), 100-109. https://doi.org/10.1016/j.yofte.2010.01.001.

Yang, H.Z. and Jiang, H.M. (2014), "Optimized tapered optical fiber for ethanol (C_2H_5OH) concentration sensing", *J. Light. Technol.*, **32**(9), 1777-1783. https://doi.org/10.1007/s11859-012-0830-7.

Yang, H.Z., Qiao, X.G., Luo, D., Lim, K.S., Chong, W.Y. and Harun, S.W. (2014), "A review of recent developed and applications of plastic fiber optic displacement sensors", *Measurement*, **48**, 333-345. https://doi.org/10.1016/j.measurement.2013.11.007.

Yang, H.Z., Ali, M.M., Islam, M.R., Lim, K.S., Gunawardena, D.S. and Ahmad, H. (2015), "Cladless few mode fiber grating sensor for simultaneous refractive index and temperature measurement", *Sens. Actuators A Phys.*, **228**, 62-68. https://doi.org/10.1016/j.sna.2015.03.001.

Yang, X.U., Luo, M., Liu, Q., Du, G. and Song, G. (2019), "PZT transducer array enabled pipeline defect locating based on time-reversal method and matching pursuit de-noising", *Smart Mater. Struct.*, **28**(7), 075019. https://doi.org/10.1088/1361-665X/ab1cc9.

Zeng, X., Dong, F.F., Xie, X.D. and Du, G.F. (2019), "A new analytical method of strain and deformation of pipeline under fault movement", *Int. J. Press. Vessel. Pip.*, **172**, 199-211. https://doi.org/10.1016/j.ijpvp.2019.03.005.

Zhu, M., Du, C.W., Li, X.G., Liu, Z.Y., Li, H. and Zhang, D.W. (2014), "Effect of AC on stress corrosion cracking behavior and mechanism of X80 pipeline steel in carbonate/bicarbonate solution", *Corros. Sci.*, **87**, 224-232. https://doi.org/10.1016/j.corsci.2014.06.028.

Zou, L., Sezerman, O. and Revie, W. (2008), "Pipeline corrosion monitoring by fiber optic distributed strain and temperature sensors", *Proceedings of the NACE International Corrosion Conference and Expo*, New Orleans, LA, USA, March.

BS